JGR Space Physics

RESEARCH ARTICLE
10.1029/2022JA031010

Special Section:
Fifteen Years of THEMIS Mission

Multiple Auroral Streamer Bundles in Conjugate Hemispheres and Multiple Near-Earth Injections

S. Tian[1], C.-P. Wang[1], L. R. Lyons[1], J. Bortnik[1], J. M. Weygand[2], J. Liu[1,2], S. Yadav[1], Q. Ma[1,3], G. D. Reeves[4], M. G. Henderson[4], and R. A. Wolf[5]

[1]Department of Atmospheric and Oceanic Sciences, University of California, Los Angeles, CA, USA, [2]Department of Earth, Planetary, and Space Sciences, University of California, Los Angeles, CA, USA, [3]Center for Space Physics, Boston University, Boston, MA, USA, [4]Los Alamos National Laboratory, Los Alamos, NM, USA, [5]Physics and Astronomy Department, Rice University, Houston, TX, USA

Key Points:

- Similar spatial and temporal development of bundles of auroral streamers is observed in conjugate hemispheres
- A streamer bundle may map to an overall bubble in the plasma sheet
- Streamers within a streamer bundle may map to narrower bubbles

Supporting Information:

Supporting Information may be found in the online version of this article.

Correspondence to:

S. Tian,
ts0110@atmos.ucla.edu

Citation:

Tian, S., Wang, C.-P., Lyons, L. R., Bortnik, J., Weygand, J. M., Liu, J., et al. (2023). Multiple auroral streamer bundles in conjugate hemispheres and multiple near-Earth injections. *Journal of Geophysical Research: Space Physics*, *128*, e2022JA031010. https://doi.org/10.1029/2022JA031010

Received 13 SEP 2022
Accepted 1 JAN 2023

Abstract The auroral streamer is a type of auroral form commonly observed during geomagnetic substorms. Previous studies suggested a coupling between auroral streamers and channels of bursty bulk flows in the plasma sheet. However, whether one flow channel can map to multiple streamers is unclear. Here, we present an event containing consecutive auroral streamer subevents. The event features similar spatial and temporal development of auroral streamers in conjugate hemispheres. In most of the subevents, we observed that what an in-space auroral camera saw as one streamer actually consisted of multiple streamers (i.e., a streamer bundle). A coordinated analysis of near-earth injections and ionospheric currents suggests that one overall flow channel (or bubble) can map to a streamer bundle. Multiple streamer bundles and thus multiple overall flow channels can occur simultaneously at different local times. Evidence supports that the overall flow channel may consist of or split into several narrower flow channels and each maps to a streamer and causes a particle injection.

Plain Language Summary Geomagnetic substorm is a complex energy release process involving many observable features in the geospace. Common substorm features include enhanced auroral activities and currents in the ionosphere, enhanced fluxes of energetic electrons and ions (injections), and localized bursty bulk flows (BBFs) in the nightside magnetosphere. It is well established that injection, BBF, and a type of aurora called auroral streamer are physically related. Here, we present an event when streamers form bundles in successive subevents and discuss how streamers and streamer bundles are related to BBF and injection. Auroral data show that these streamer bundles developed similarly in both hemispheres. We show observational evidence that a streamer bundle maps to an overall BBF and streamers within a bundle map to narrower BBFs.

1. Introduction

Auroral streamers have been widely studied for decades (cf. Forsyth et al., 2020, and references therein). Traditionally, these refer to the north-south aligned aurora (e.g., Henderson, 1994; Nakamura et al., 1993), to be distinguished from the east-west aligned auroral arcs. However, the alignment is no longer considered a key descriptor. Instead, the critical aspect of the definition of an auroral streamer is the dynamic development away from the origin toward the equatorward boundary of the auroral oval (Forsyth et al., 2020). There are also poleward moving streamers reported (W. W. Liu et al., 2008). In this study, auroral streamers or streamers refer to aurora features that are approximately north-south aligned or extend equatorward, that is, following either the traditional or the renewed definition.

Auroral streamers and bursty bulk flows (BBFs) have long been suggested to correlate (Henderson et al., 1998; Nakamura et al., 1993). According to our current understanding (Cross-Scale Coupling and Energy Transfer in the Magnetosphere-Ionosphere-Thermosphere System, 2022, and references therein), an auroral streamer is coupled to a channel of BBF (Angelopoulos et al., 1994; Baumjohann et al., 1990) occurring in the plasma sheet. The equatorward development of the streamer corresponds to the earthward development of the flow channel (Zesta et al., 2000). The streamer couples to the flow channel through a pair of upward and downward field-aligned currents (FACs) (Nakamura et al., 2001; Sergeev et al., 2000), which has been predicted by the bubble model (Chen & Wolf, 1993) for the flow channel. In this study, we will use bubble and flow channel interchangeably. The ionospheric signature of the upward (downward) FAC is a counterclockwise (clockwise) Hall

current loop (Kauristie et al., 1996). The predicted ionospheric current signature has been observed (Kauristie et al., 1996; Weygand et al., 2022).

The earthward moving head of the flow channel is associated with a sudden enhancement of the magnetic field tilt angle or B_z, that is, the dipolarization front (DF) or dipolarizing flux bundle (DFB) (J. Liu et al., 2013; Nakamura et al., 2002; Runov et al., 2009). The DFB is also associated with the injection of keV electrons and ions in the near-earth region (Kivelson et al., 1980; McIlwain, 1974; Runov et al., 2013). Streamers are also observed to be associated with localized impulsive injections (Henderson, 2009; Sergeev et al., 1999). These observations further elaborate on the coupling between the streamer and the flow channel.

Previous studies on streamers often see them appear as or develop into bundles (Henderson et al., 1998; Pritchett et al., 2014; Rostoker et al., 1987). This motivates a coordinated study to inspect whether a streamer bundle or the streamer within a bundle corresponds to a BBF. In addition, in this study, we use ground and in-space auroral cameras to inspect the inter-hemispheric development of streamers, which has not yet been extensively studied except for several examples published by Sato et al. (2012, 2015). Yet these inter-hemispheric comparisons are only within a limited field of view (∼9 deg). Here we observed a similar spatial and temporal development in the northern and southern hemispheres on a much larger scale. In our event, what the in-space camera observed as one streamer was often a streamer bundle as resolved by the ground cameras. We further utilize the injection and ionospheric current measurements to study how the streamer bundles are related to injections and flow channels. In the rest of this study, we briefly introduce the instrumentation in Section 2 and show the observations in Section 3. Discussion and conclusions are presented in Section 4 and Section 5, respectively.

2. Instrumentation

In this study, we study events when the nightside auroral ovals in the conjugate hemispheres were simultaneously monitored by the ultraviolet imager (UVI) onboard the Polar spacecraft in the southern hemisphere and by the "Time History of Events and Macroscale Interactions during Substorms" (THEMIS) network of ground magnetometers (GMAGs) and all-sky imagers (ASIs) in northern America. Polar UVI (Torr et al., 1995) can typically cover the entire nightside auroral oval at a cadence of ∼37 s. The ASIs (Mende et al., 2008) can record the aurora at a much higher cadence of 3 s. The spatial resolution of the pixels of Polar UVI was about 30 km in this event (6×10^{-4} rad per pixel, the geocentric distance of Polar was 7–9 Re). The spatial resolution of the pixels of THEMIS ASIs is typically 1–5 km. Combining the two types of auroral measurement allows us to monitor the global morphology of the auroral oval with Polar UVI and resolve finer auroral structures with ASIs. The ASI data in the event for this study were contaminated by the moon. A moon removal technique is developed and explained in Appendix A. The moon is successfully removed as shown in Supporting Information Movie S1.

The THEMIS GMAGs (Russell et al., 2008) measure the magnetic field perturbations over Northern America. The technique of spherical elementary current system (SECS) can be used to derive the ionospheric current from the GMAG measurements (Amm & Viljanen, 1999; Vanhamäki & Juusola, 2020). The SECS (Weygand, 2009a, 2009b; Weygand et al., 2011) data (10 s cadence) contain current components that are vertical and horizontal relative to the ground. Around the auroral latitudes, the background magnetic field is approximately perpendicular to the ground. Hence, the SECS vertical and horizontal current data are good estimates of the parallel and perpendicular currents respectively. The parallel currents are also referred to as the field-aligned currents (FACs).

In our auroral event, in-situ features studied include particle injection and dipolarization. The LANL (Los Alamos) spacecraft measures the e− and H+ fluxes from 50 keV to above 1 MeV (Bame et al., 1993; Belian et al., 1992). Contaminated LANL H+ flux channels are excluded, including those around 60, 89, and 577 keV. The THEMIS solid-state telescope measures the electron and ion fluxes from 25 keV to above 1 MeV (Angelopoulos, 2008). The keV fluxes from LANL and THEMIS are used to study dispersionless and dispersive injections. The Geostationary Operational Environmental Satellite (GOES) (Singer et al., 1996) and THEMIS (Auster et al., 2008) magnetic fields are used to study the dipolarizations.

3. Observations

During the 3 hr from 06:00 UT to 09:00 UT on 19 January 2008, eight auroral subevents occurred successively in a 10–20 min cadence. Each one was associated with an increase of the auroral electrojet (AE) and/or Supermag

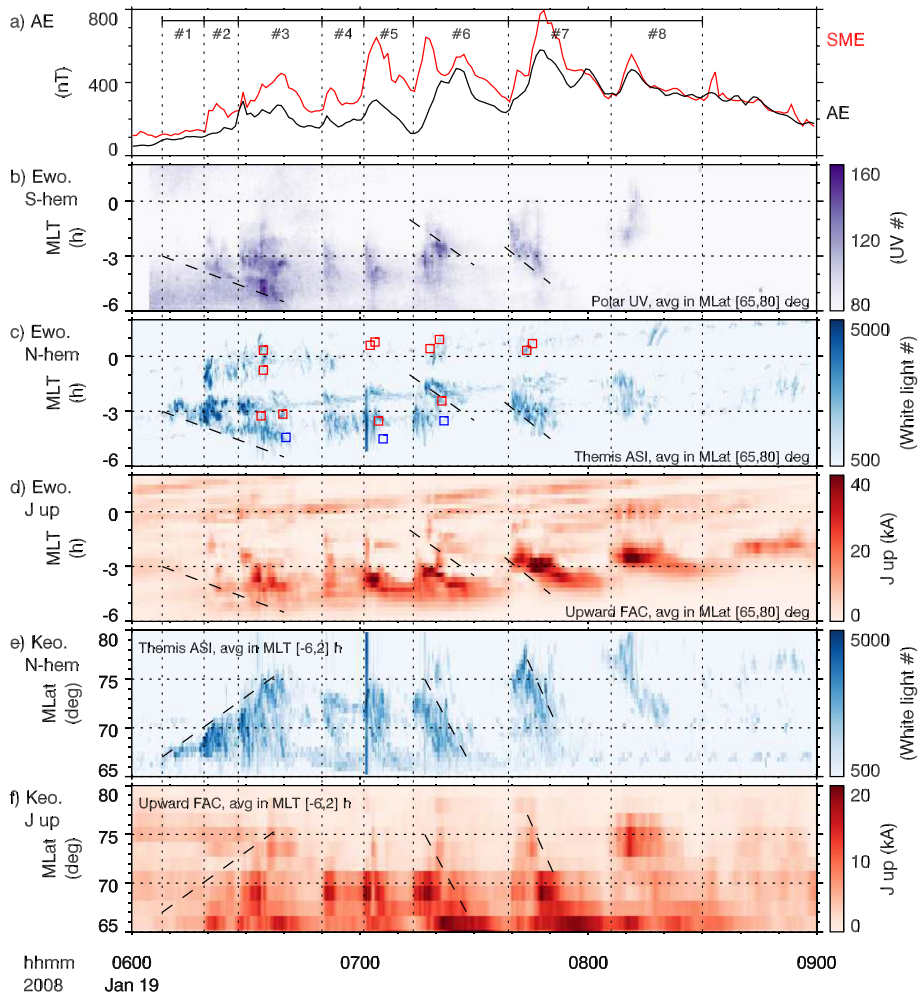

Figure 1. Similar development of eight successive auroral activities was observed in the southern and northern hemispheres. Panel a shows the auroral electrojet (AE) and Supermag electrojet (SME) indices during 3 hr from 06:00 to 09:00 UT on 19 January 2008. Panels b and c show the ewogram for the auroral oval in the southern and northern hemispheres as measured by the Polar ultraviolet imager and Time History of Events and Macroscale Interaction during Substorms (THEMIS) all-sky imagers (ASIs). The red (blue) squares mark the electron (ion) injection region determined in Section 3. Panel d shows the ewogram for the upward current derived from the ground magnetometer data in the northern hemisphere. Panels e and f show the keogram of the aurora and upward current in the northern hemisphere. During the event, we observed a very similar azimuthal evolution of the aurora in conjugate hemispheres. Polar latitudinal evolution (keogram) is not compared because the data contain instrumental uncertainty in latitudes.

electrojet indices (Figure 1a). Note that the AE index missed some of the subevents (e.g., subevent #2) probably because AE uses fewer ground stations. The vertical dotted lines in Figure 1a mark the start of the subevents. To illustrate what auroral forms are observed and how they evolve, we present the aurora measurements from two perspectives: Figure 1 focuses on the temporal evolution of the aurora versus the magnetic local time (MLT, ewogram) and versus the magnetic latitude (MLat, keogram) during the entire event and Figure 2 presents several snapshots of the auroral oval to show the auroral forms. In Figure 1, the ewogram is averaged over the entire auroral latitudes (65–80 deg MLat) and the keogram is averaged over the MLT range from −6 (18) to 02 MLT. A full movie of the aurora and the ionospheric current is included in Movie S1 in the Supporting Information.

As an example of auroral streamers, the ASI data (Panel b) in Movie S1 in the Supporting Information shows the equatorward development (from 75 to 66 deg MLat) of auroral streamers around −2 (22) MLT around 07:20 UT. These streamers are shown in Panel b-3 in Figure 2. The equatorward development is clear in the keogram (Panel e in Figure 1, the dashed line during subevent #6). In addition, a westward motion is shown in the ewogram (Panel c in Figure 1, the dashed line during subevent #6).

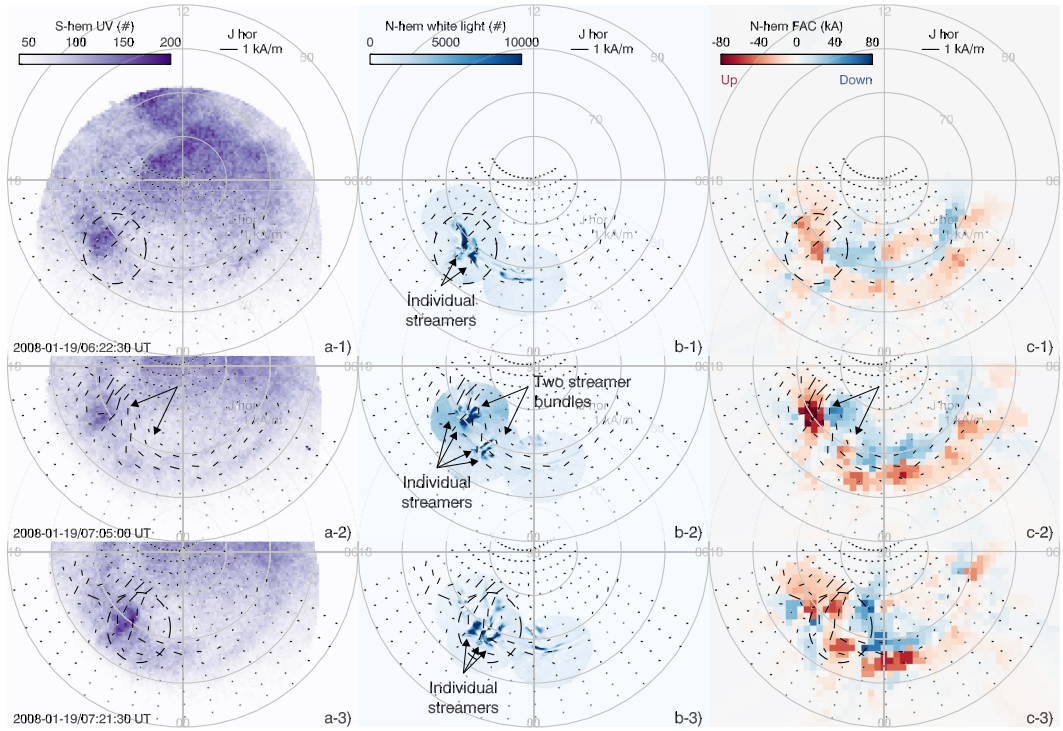

Figure 2. Snapshots of the auroral oval observed in the southern and northern hemispheres. Polar ultraviolet imager (UVI) covered the southern hemisphere (Panels a-1 to a-3). Three Time History of Events and Macroscale Interaction during Substorms (THEMIS) all-sky imagers (ASIs) (FSIM, GILL, and INUV) covered a large fraction of the northern hemisphere (Panels b-1 to b-3). In Panels c-1 to c-3, we use the vertical currents to estimate the upward and downward field aligned currents (FAC). The horizontal currents are overplotted in all panels at each snapshot time. Within the areas circled or pointed, the auroral structures observed by Polar UVI are resolved as multiple streamers by the THEMIS ASIs. The streamers corresponded to the upward FAC.

From the ewograms in Figure 1, the eight auroral subevents were in general evolving symmetrically in local time in the southern hemisphere (Panel b) and northern hemisphere (Panel c). For example, we observed a gradual westward expansion from 06:10 UT to 06:40 UT (indicated by the dashed lines in Panels b and c). From 07:00 UT to 08:00 UT, we marked two additional westward motions of the aurora. In all these examples, the azimuthal motions in the conjugate hemispheres occurred simultaneously around the same local time. Note that the auroral intensities of Polar UVI and THEMIS ASI are not directly comparable to each other because UVI observes the ultraviolet range whereas ASI observes the white light.

Figure 1 also compares the aurora and upward currents in the northern hemisphere (Panel d). Since discrete aurora like streamers corresponds to the upward current, we expect them to develop similarly. As shown in the ewograms (Panels c and d) and keograms (Panels e and f), regardless of the much lower spatial resolution of the current data, the upward current, in general, followed similar azimuthal and latitudinal motions as the aurora. Note that the upward current and aurora do not match exactly in evolution. For example, from 07:50 UT to 08:00 UT, it is clear that the upward current penetrated to lower latitudes (Panel f) and remained strong after the aurora dimmed (Panels e and f). The Polar UVI images in this event are smeared out primarily in latitude due to the wobble of the camera. However, the wobble does not change the average location of a certain auroral structure. The auroras observed by Polar UVI can be seen to be around the same latitude as those observed by ASIs (Figure 2).

Figure 2 shows several snapshots of the auroral oval in the southern hemisphere (Polar UVI, Column a) and northern hemisphere (THEMIS ASI, Column b) during three of the subevents shown in Figure 1 (subevents #2, #5, and #6). Column c shows the FACs where red is for upward currents and blue is for downward currents. In each row, we plot the northern hemisphere horizontal currents as vectors, where the grids are the starting points of the vectors. Column a shows that a streamer was observed by UVI around −3 (21) MLT in all the snapshots. Compared to Column b, it is clear that each of the Polar streamers was indeed a group of streamers as resolved

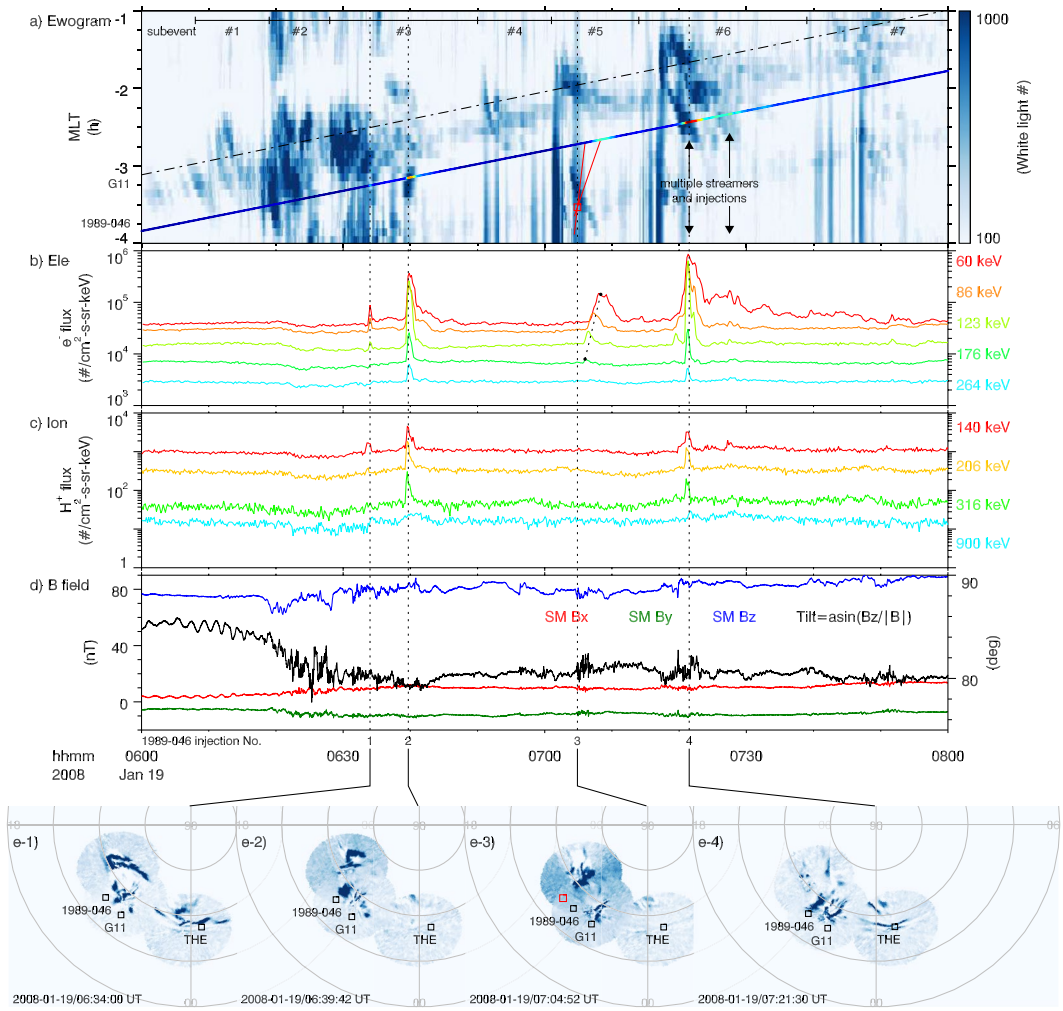

Figure 3. The injection observation at LANL 1989-046 and magnetic field at Geostationary Operational Environmental Satellite (GOES) 11 during the 19 January 2008 event. Panel a shows the expanded version of the ewogram of the all sky imagers (ASIs). The track of LANL 1989-046 is overplotted and color-coded by the electron flux intensity at 60 keV. The track of GOES 11 is overplotted as the dot-dashed line. For the dispersive injection around 07:15 UT, when and where the corresponding dispersionless injection occurred are estimated by tracing the electron's curvature and gradient drifts in the T89 magnetic field model (Tsyganenko, 1989). In Panel a, the drift velocities at 60 and 176 keV are marked by the two red lines and the time and MLT of the estimated injection region are represented by the red square. Panels b and c show the LANL 1989-046 electron and ion fluxes at keV energy channels. The sloped dotted line around 07:15 UT marks the peaks of electron flux from 60 to 176 keV. Panel d shows the GOES 11 magnetic field components in the solar magnetic (SM) coordinate system and its tilt angle (black). Panel e shows four ASI snapshots at the times of the vertical dashed lines. All four injections seen by LANL were associated with either auroral streamers or streamer bundles. The third injection was dispersive, which corresponds to a dispersion region around −3.5 (20.5) MLT and thus the streamer bundle westward of LANL 1989-046.

by the THEMIS ASIs. The streamers are in general around the same MLT and latitude as the upward currents (Column c), which has been shown in Figure 1. It is interesting to note that at 07:05 UT (Row 2), the ASIs observed two streamer bundles around 21 and 22 MLT (Panel b-2). UVI clearly observed the brighter one around 21 MLT. For the weaker streamer bundle around 22 MLT, based on the ASI data, we believe that it corresponds to the weak enhancement in UVI around 22 MLT (arrows in Panel a-2).

3.1. Injections in the Pre-Midnight Sector

Figure 3 shows the pre-midnight portion of the aurora ewogram in the northern hemisphere and the associated LANL (1989-046) keV particle measurements. The ewogram in Figure 3a is averaged over [65,75] deg

MLat. This is a smaller range than that used in Figure 1c ([65,80] deg MLat), to eliminate the effect of poleward arcs because we will focus on the streamers. LANL 1989-046 observed a dispersive electron injection during subevent #5. We trace the gradient and curvature drifts of these electrons in the T89 model magnetic field (Tsyganenko, 1989) and obtained an electron injection region located around −3.5 (20.5) MLT (red box in Panel a), where the electrons would be dispersionless. In Panel e−3, the electron injection region is marked by the red square using the determined MLT. The MLat is randomly chosen because mapping uncertainty and penetration depth are unknown. Nevertheless, the local time of the electron injection region was around the streamer bundle around −3.5 (20.5) MLT (Panels a and e−3). LANL 97A was eastward of this streamer bundle and observed dispersive proton injection (Figure S2 in the Supporting Information S1). The tracing results of the dispersive ion (blue square) and electron (red square) injections are marked in Figure 1 Panel c. They were both close to the local time of the streamer bundle around −3.5 (20.5) MLT (Panel e−3 in Figure 3). These results suggest that the streamer bundle corresponded to an injection region, which is consistent with previous studies on streamer and injection (Henderson, 2009; Sergeev et al., 1999).

In addition to the dispersive electron injection, LANL 1989-046 also observed three dispersionless peaks in both the electron and ion fluxes (Figure 3 Panels b and c). These peaks were observed when streamer bundles drifted over LANL 1989-046's MLT (Panel a). Although dispersionless flux peaks may be caused by either actual injections or magnetic field dipolarizations, based on the fact that the dispersive injection was clearly related to a streamer bundle, we argue that these dispersionless peaks were actual dispersionless injections and thus LANL 1989-046 observed four injections in total, as labeled in Figure 3. From injection 4, we can see that there were multiple peaks when multiple streamers within a bundle drifted over LANL 1989-046 (arrows in Panel a). Thus each streamer within a streamer bundle is likely to have its own injection region.

3.2. Injections Around Midnight

During subevents #3, #5, and #6, THD, THE, and THA also observed dispersive electron injections, which were all traced to injection regions around midnight (Figure 1 Panel c). Therefore these injections are related to the auroral activities around midnight. They are separate injections from the injections associated with the streamer bundles in Section 3.1. Since this study focuses on the streamer bundles, we will not further discuss the THEMIS injections. The tracing of these injections is shown in Figure S3 in the Supporting Information S1.

4. Discussion

We have shown the successive subevents of auroral activities on 19 January 2008. As shown in Movie S1 in the Supporting Information, all subevents after 06:19 UT contained auroral streamers in the pre-midnight sector. This study primarily focuses on these streamers. The Polar UVI and THEMIS ASI recorded similar spatial and temporal development of the auroral streamers in conjugate hemispheres. By similar development, we mean that an auroral streamer (or a streamer bundle) in one hemisphere has its counterpart in the other hemisphere around similar latitudes and longitudes. In addition, they both brighten and dim almost simultaneously and follow similar latitudinal and longitudinal motions. The similar development of streamers in conjugate hemispheres is consistent with our current understanding that the coupling between a flow channel in the plasma sheet and the ionosphere would be similar in both hemispheres.

4.1. Inter-Hemispheric Symmetry

Sato et al. (2012, 2015) showed interhemispheric comparisons of streamers at two magnetically conjugate all-sky imagers (∼9 deg field of view). The authors observed mixed results—streamers are similar in some cases but are different in other cases. In our study, since streamers in the consecutive subevents exhibited similar development in both hemispheres, we suggest that this is the normal scenario and different development may indeed occur but we expect this to be less often. In addition, since the conjugate all-sky imagers have a limited field of view, the difference may be due to the limited spatial coverage. Our study can avoid this issue because the Polar UVI has a much larger field of view.

The most noticeable motion of the streamers is the equatorward motion. However, it is interesting to note that both Polar UVI and THEMIS ASI observed similar azimuthal motions of the auroral streamers (e.g., subevents #5, #6, and #7 in Panels b and c in Figure 1). This motion, based on the expanded ewogram in Panel a in Figure 3, was about 2–3 deg/min. The ewograms further show that neither the streamer nor the upward current significantly

expanded in longitudinal width during the azimuthal motion (e.g., the dashed lines for subevents #6 and #7 in Panels b, c, and d in Figure 1).

Given the coupling between streamers and flow channels as discussed in Section 4.2, this suggests that the flow channel in the plasma sheet moved azimuthally but did not noticeably expand in width. Therefore, the azimuthal motion of the streamer and the presumably coupled flow channel is an azimuthal drift instead of some azimuthal expansion, for example, due to the magnetic flux pileup (Baumjohann et al., 1999). We suggest that the azimuthal drift is due to global convection. Based on previous statistical studies, global convection is away from midnight (Miyashita et al., 2020; Wang et al., 2006). The speed is on the order of several 10s km/s within the transition region (<12 Re). This is consistent with the azimuthal drift of the streamers. Similar azimuthal drifts of flow channels can be seen in MHD simulations (e.g., Eshetu et al., 2019). Another possible factor affecting the auroral motion is the changes in mapping due to the FAC and dipolarization associated with the flow channels.

4.2. Streamer and Flow Channel

Combining the Polar UVI and THEMIS ASI streamer observations, we can see that what Polar saw as one streamer is often indeed a streamer bundle (e.g., Panels a-1, b-1, a-3, and b-3 in Figure 2). Although UVI and ASI are different in wavelength and thus do not necessarily capture the same features of the aurora, the difference here is probably due to the low spatial resolution of UVI. An interesting question arises because although many early works suggest a one-to-one correspondence for streamer injection (Henderson, 2009; Sergeev et al., 1999) and streamer-flow channel (Nakamura et al., 2001; Sergeev et al., 2000), the correspondence of streamer bundle has not been discussed. This is especially interesting since in our event one Polar streamer can indeed be a streamer bundle when viewed in high spatial and temporal resolution.

The observations in our event suggest that a streamer bundle maps to one overall flow channel. Section 4.3 discusses the possible splitting of the overall flow channel into narrower ones. Panel b-2 in Figure 2 shows that two streamer bundles were observed around 07:05 UT around −3.5 (20.5) and −2 (22) MLT. The observed FAC distribution contained two pairs of upward-downward FACs (Panel c-2 in Figure 2). Previous studies have shown that one flow channel generates a pair of upward-downward FACs (Kauristie et al., 1996; Wang et al., 2018, 2020; Weygand et al., 2022). The fact that the two FAC pairs were observed at different MLTs but at similar latitudes suggests that this FAC pattern is caused by two spatially separated flow channels.

To test this plausibility, we use the UCLA version of the Rice Convection Model (UCLA-RCM) to simulate the FAC pattern due to two flow channels (twin bubbles). Gkioulidou et al. (2012) describe the UCLA-RCM and the differences between the UCLA-RCM and the original RCM. Here we use the UCLA-RCM to conduct a simulation run for twin bubbles separated by 2 hr in MLT (at 23 and 01 MLT). The setup of the simulation is explained in Appendix Appendix B. Figure 4 shows a snapshot 10 min after the bubbles were initiated. A full movie of the simulation is in Movie S2 in the Supporting Information. Two bubbles, about 2–4 Re wide, are characterized by, for example, high velocities (Panel a-2) and high ion temperatures (Panel a-5). They were associated with two pairs of upward and downward FACs in the ionosphere (Panel b). The FAC pattern from the simulation (Panel b) is qualitatively similar to the observed pattern (Panel c). Therefore, we conclude that it is plausible that there were two flow channels and that they mapped to the two observed streamer bundles.

4.3. Streamer Bundle and Possible Bubble Splitting

In Section 4.2, we showed that a streamer bundle probably maps to one bubble, and based on the UCLA-RCM simulation, the bubble would be 2–4 Re wide, which is the typical size (J. Liu et al., 2013). Similar streamer bundles instead of single streamers were observed in many of the subevents, for example, in subevents #3, #5, and #6 (cf. Movie S1 in the Supporting Information). Among them, subevent #6 contained the best injection conjunction because its streamers are clear and LANL 1989-046 was right around the streamers' MLT. In Section 3.1, we showed that the largest peak of the electron and ion injections at LANL 1989-046 (Panels b and c in Figure 3) was associated with the westmost streamer (Panel e-4 in Figure 3). The later smaller peaks were associated with the streamers further east within the streamer bundle. This means that each streamer within that streamer bundle should map to one injection region. From simulation and observations (Gabrielse et al., 2017; Runov et al., 2013), each flow channel should cause an injection. Therefore, although in Section 4.2 we showed that one streamer bundle maps to an overall flow channel, each streamer within the streamer bundle should correspond to a narrower flow channel. This is illustrated in Figure 5.

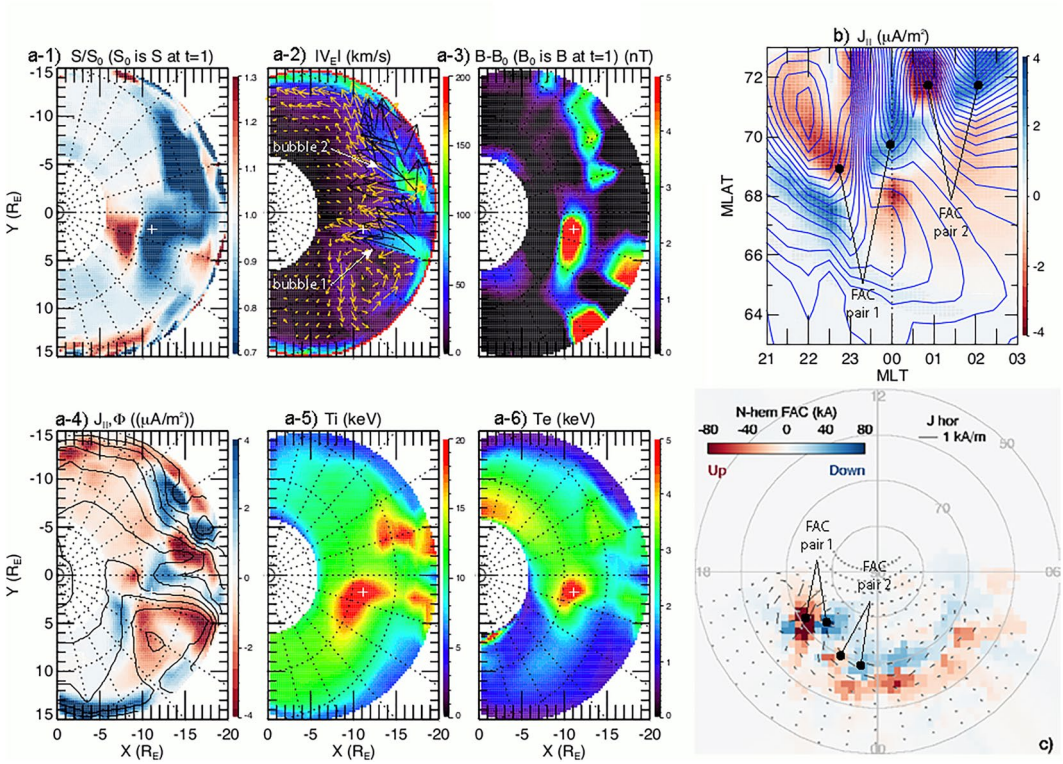

Figure 4. UCLA-Rice Convention Model simulation results for twin bubbles launched at 23 and 01 MLT. Panels on the left show (a-1) normalized entropy, (a-2) velocity vectors and magnitude (color), (a-3) magnetic field, (a-4) parallel current (color), and electric potential (contour), (a-5) ion temperature, and (a-6) electron temperature. Panel b shows the ionospheric field-aligned currents (FACs) (color) and the electric potential (contour). Panel c shows the measured FACs (same as Panel c-2 in Figure 2).

In the ewogram either in Figure 3a or Movie S1 in the Supporting Information, all streamers within a streamer bundle evolved almost simultaneously. This suggests that the narrower flow channels that the streamers may map to probably also evolve simultaneously. Although the overall flow channel may either split into or consist of the narrower flow channels, we speculate that splitting is more likely because it would naturally explain the simultaneity. Limited by spatial resolution, we can only observe the FAC pattern of the overall flow channel, but it probably consists of the wedgelets of the narrower flow channels (J. Liu et al., 2015). Some simulations also suggest the splitting of an overall flow channel into narrower ones (Birn et al., 2019; Pritchett et al., 2014). The

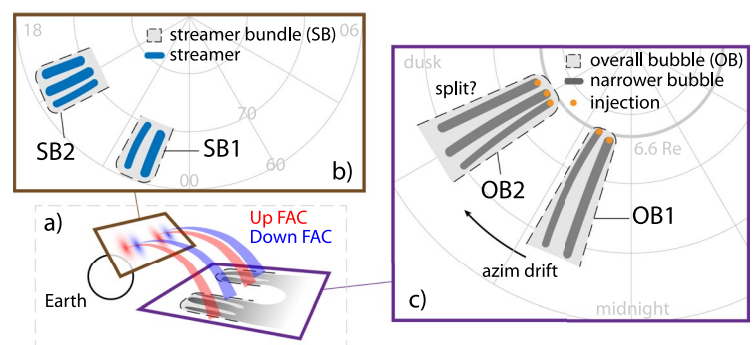

Figure 5. The schematic summarizes the observed multiple streamer bundles, up-down field aligned current (FAC) pairs, injections, and the conjectured multiple narrower flow channels (bubbles) within the overall bubbles. A streamer bundle maps to an overall bubble of 2–4 Re wide through a pair of up-down FAC. Streamers within a streamer bundle map to narrower bubbles, presumably through wedgelets. The overall bubble either splits into or consists of narrower bubbles. Splitting is more likely based on simultaneity and previous studies.

overall earthward flow channels are suggested to be generated in the tail reconnection and propagate earthward due to interchange-type of instabilities (Forsyth et al., 2020, and references therein). Based on our observations, the overall earthward flow channel seems to further evolve (split) into narrower flow channels. While whether such splitting occurs and the splitting physics remain questions for future research, we note that the ballooning/interchange instability has been theoretically proposed to lead to a breakup of flow channels and spatial structuring of auroral streamers (Pritchett et al., 2014).

5. Conclusions

In conclusion, we studied a 3-hr auroral event that features consecutive subevents of streamers and streamer bundles. Conjugate observations in a global field of view show that the auroral streamers develop similarly in both hemispheres, that is, corresponding auroral streamers evolve around similar times and locations (latitude and MLT) in the northern and southern hemispheres. We suggest that similar development is the normal scenario and that different development might be occasional. In many of the streamer subevents, streamer bundles, in which several streamers appear simultaneously around a similar MLT, are often observed. Based on the comparison between the streamer bundle and FAC pattern, we conclude that each streamer bundle corresponds to an overall flow channel that is 2–4 Re wide. In our event, multiple streamer bundles appeared simultaneously, suggesting multiple overall flow channels in the tail. We show observational evidence for narrower flow channels within the overall flow channel. Coordinated comparisons between the azimuthal drift of the streamers and LANL injections showed that each streamer within a streamer bundle has its own injection region and thus probably its own narrower flow channel.

Appendix A: Moon Removal Technique for ASI

All-sky imagers observe the aurora from the ground and thus are inevitably contaminated by the moon. Fortunately, the moon moves much slower than auroral streamers within the field of view of ASIs. Therefore, although the brightness of a certain pixel of the ASI image consists of both the contribution from the moon and streamer, the moon's contribution is a slowly varying background and thus can be removed. Here we describe the algorithm.

The all-sky imager data is a series of images of 256 × 256 pixels. For n frames of images, the data is an array of [n, m, m]. Instead of processing the image per frame, we consider the brightness of a fixed pixel, which is an array of [n]. Here, we define the raw images as $r_{m,m}[n]$, where $m = 256$. We use i, j, k to iterate among [m, m, n]. For example, $r_{i,j}[n]$ is the raw brightness at the pixel [i, j], where $i, j \in [0, 256)$; $r_{m,m}[k]$ is the raw image at the frame k, where $k \in [0, n)$.

Figure A1 shows examples of $r_{i,j}[n]$ with and without the moon. We can classify the pixels into 3 categories.

1. Edge pixels. $r_{i,j}[n]$ is almost a constant and the value is small (green).
2. Center pixels without the moon. $r_{i,j}[n]$ may contain fluctuations due to auroral forms. The stable arc causes a fluctuation on the order of 10–20 min (red in Panel b-1). The streamer causes a fluctuation on the order of several min (purple in Panel b-2).
3. Center pixels contaminated by the moon. $r_{i,j}[n]$ saturate within the moon's surface (red in Panel b-2, before 07:24 UT) and contain a large and slowly varying background within the moon's glow (after 07:24 UT).

Therefore, we can simply remove the slowly varying background to remove the moon and thus extract the signal related to auroral forms.

There are multiple methods to calculate this slowly varying background, which we call the "baseline" hereafter. We use $\beta_{i,j}[n]$ for the baseline of the raw brightness $r_{i,j}[n]$. A simple method is to extract $\beta_{i,j}[n]$ by smoothing $r_{i,j}[n]$ over a window on the order of 10–20 min. The simple method works well with fast-moving auroral structures like streamers and discrete arcs. Because this study focuses on streamers (e.g., purple line in Panel b-2 in Figure A1), the simple method (window of 15 min) is used.

The simple method does not work well with stable arcs (e.g., red line in Panel b-1 in Figure A1), because a simple smoothing will attribute a significant portion of the auroral's signal to the baseline. To solve this problem, we developed a more complicated method to calculate the baseline, which

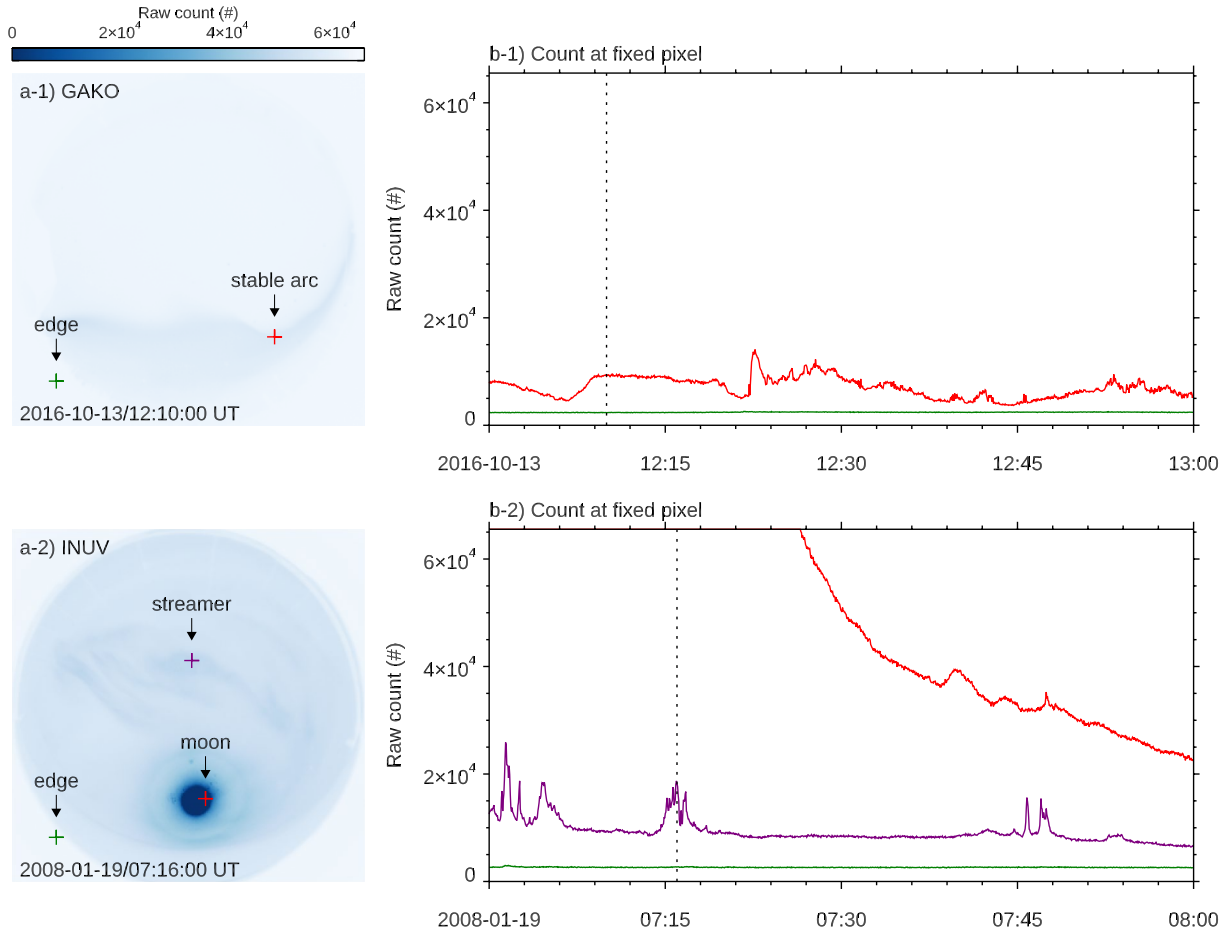

Figure A1. Examples of the all sky imager images at selected times (Panels a-1 and a-2) and the raw brightness at selected pixels (Panels b-1 and b-2). The selected times are marked by the vertical dashed line in Panels b-1 and b-2. The selected pixels are marked by + in Panels a-1 and a-2 and color-coded to differentiate them.

works with generic THEMIS ASI data based on our tests on many auroral events. In this method, we use three characteristic baselines to approximate the raw brightness: the raw brightness itself $\left(\beta^1_{i,j}[n]\right)$, the baseline at the window size of 180 s $\left(\beta^2_{i,j}[n]\right)$, and the minimum value of the raw brightness $\left(\beta^3_{i,j}[n]\right)$. They correspond to the window size of w_s, where $s = 1, 2, 3$. w_1 is 3 s (the data rate), w_2 is 180 s, and w_3 is infinity (we set it as 1,800 s). We then calculate a background brightness $b_{i,j}[k]$ defined as $b_{i,j}[k] = \text{interpol}\left(\beta^{w_s}_{i,j}[n], w_s, w_{i,j}[k]\right)$, where $w_{i,j}[k] = 3 + 2\exp(5.5655 - r_{i,j}[k] \times m_{i,j}[k] \times 10^{-4})$ is the "adaptive width." It decreases for a larger raw brightness because this indicates that the pixel is closer to the moon and thus we want the baseline to be close to the raw brightness. In addition, it is modulated by the "moon weight" $m_{i,j}[k] = 1 + 2\exp(1 - \theta_{i,j}[k]/2.5)$, where $\theta_{i,j}[k]$ is the angle between the moon and a given pixel $[i, j]$ at a certain frame k (in deg). The moon weight helps to eliminate unnecessary modification to pixels that are far away from the moon. Note that where the moon appears in the ASI is only crudely predicted and that the moon's glow is much larger than the moon's surface. This is why the moon's position is indirectly used through the moon weight. With the background calculated for all pixels and frames, we get the moon-calibrated data by removing the background brightness from the raw brightness $c_{m,m}[n] = r_{m,m}[n] - b_{m,m}[n]$. Figure A2 shows the examples of the raw brightness ($r_{m,m}[k]$, Column 1), background brightness ($b_{m,m}[k]$, Column 2), and calibrated brightness ($c_{m,m}[k]$, Column 3) at a certain frame k. It also shows the raw and background brightness at certain pixels $[i, j]$ ($r_{i,j}[n]$ and $b_{i,j}[n]$, Panels b and d). A full description of the algorithm is available at Tian (2022).

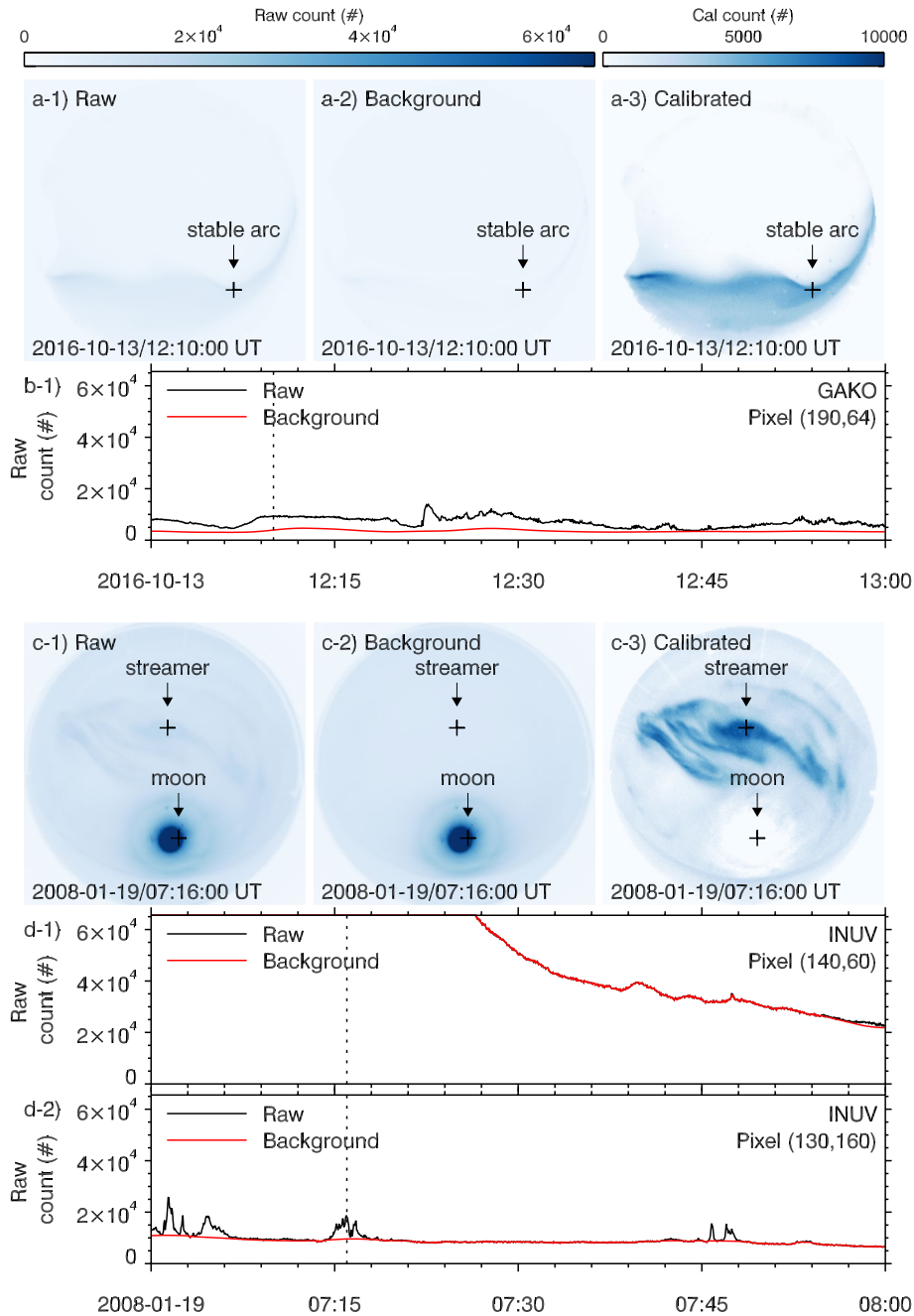

Figure A2. Examples showing the raw, background, and calibrated brightness at certain frames or at certain pixels.

Appendix B: The UCLA-RCM Simulation Setup

We modify the single bubble setup described in Wang et al. (2018 2020) to specify the RCM tail boundary conditions for the two bubbles (see Figure S1 in Supporting Information S1): (a) The two bubbles are initiated simultaneously with one at 23 and the other at 01 MLT (Panel a in Figure S1 in Supporting Information S1), (b) each bubble is imposed by increasing the ion and electron temperatures within a 0.5 MLT width at the tail boundary by a factor of 3 and decreasing their densities by a factor of 6 (Panel b in Figure S1 in Supporting Information S1), and (c) both bubbles are turned on for ∼10 min from $t = 1 - 10$ min (Panel c in Figure S1 in Supporting Information S1).

Data Availability Statement

The LANL data are available on request. The LANL data used in this study is posted at https://doi.org/10.5281/zenodo.7076361. The GOES data are available at https://cdaweb.gsfc.nasa.gov/pub/data/goes/. The THEMIS data are available at https://cdaweb.gsfc.nasa.gov/pub/data/themis/. The SECS data are available at https://cdaweb.gsfc.nasa.gov/pub/data/aaa_special-purpose-datasets/spherical-elementary-and-equivalent-ionospheric-currents-weygand/.

Acknowledgments
The authors would like to thank the following mission teams for providing the data used in this study including LANL, GOES, and THEMIS (spacecraft, ASI, and GMAG). The work at UCLA has been supported by NSF Grant 2055192, NASA Grants 80NSSC20K1314, 80NSSC22K0749, 80NSSC19K0306, 80NSSC22K1027, and AFOSR FA9559-16-1-0364. JB acknowledges the support from NASA HSR Grant 80NSSC18K1227. JL would like to thank NASA grants: 80NSSC22K0749, 80NSSC22K0751, 80NSSC21K1407, 80NSSC20K1314, 80NSSC20K1316, and NSF grant AGS-2055192.

References

Amm, O., & Viljanen, A. (1999). Ionospheric disturbance magnetic field continuation from the ground to the ionosphere using spherical elementary current systems. *Earth Planets and Space*, *51*(6), 431–440. https://doi.org/10.1186/BF03352247

Angelopoulos, V. (2008). The themis mission. *Space Science Reviews*, *141*(1–4), 34. https://doi.org/10.1007/s11214-008-9336-1

Angelopoulos, V., Kennel, C. F., Coroniti, F. V., Pellat, R., Kivelson, M. G., Walker, R. J., et al. (1994). Statistical characteristics of bursty bulk flow events. *Journal of Geophysical Research*, *99*(A11), 21257–21280. https://doi.org/10.1029/94JA01263

Auster, H. U., Glassmeier, K. H., Magnes, W., Aydogar, O., Baumjohann, W., Constantinescu, D., et al. (2008). The themis fluxgate magnetometer. *Space Science Reviews*, *141*(1–4), 235–264. https://doi.org/10.1007/s11214-008-9365-9

Bame, S. J., McComas, D. J., Thomsen, M. F., Barraclough, B. L., Elphic, R. C., Glore, J. P., et al. (1993). Magnetospheric plasma analyzer for spacecraft with constrained resources. *Review of Scientific Instruments*, *64*(4), 1026–1033. https://doi.org/10.1063/1.1144173

Baumjohann, W., Hesse, M., Kokubun, S., Mukai, T., Nagai, T., & Petrukovich, A. A. (1999). Substorm dipolarization and recovery. *Journal of Geophysical Research*, *104*(A11), 24995–25000. https://doi.org/10.1029/1999JA900282

Baumjohann, W., Paschmann, G., & Lühr, H. (1990). Characteristics of high-speed ion flows in the plasma sheet. *Journal of Geophysical Research*, *95*(A4), 3801–3809. https://doi.org/10.1029/JA095iA04p03801

Belian, R. D., Gisler, G. R., Cayton, T., & Christensen, R. (1992). High-z energetic particles at geosynchronous orbit during the great solar proton event series of october 1989. *Journal of Geophysical Research*, *97*(A11), 16897–16906. https://doi.org/10.1029/92JA01139

Birn, J., Liu, J., Runov, A., Kepko, L., & Angelopoulos, V. (2019). On the contribution of dipolarizing flux bundles to the substorm current wedge and to flux and energy transport. *Journal of Geophysical Research: Space Physics*, *124*(7), 5408–5420. https://doi.org/10.1029/2019JA026658

Chen, C. X., & Wolf, R. A. (1993). Interpretation of high-speed flows in the plasma sheet. *Journal of Geophysical Research*, *98*(A12), 21409–21419. https://doi.org/10.1029/93JA02080

Cross-scale coupling and energy transfer in the magnetosphere-ionosphere-thermosphere system. (2022). *Cross-scale coupling and energy transfer in the magnetosphere-ionosphere-thermosphere system*. Elsevier. https://doi.org/10.1016/C2019-0-00526-2

Eshetu, W. W., Lyon, J. G., Hudson, M. K., & Wiltberger, M. J. (2019). Simulations of electron energization and injection by bbfs using high-resolution lfm mhd fields. *Journal of Geophysical Research: Space Physics*, *124*(2), 1222–1238. https://doi.org/10.1029/2018JA025789

Forsyth, C., Sergeev, V. A., Henderson, M. G., Nishimura, Y., & Gallardo-Lacourt, B. (2020). Physical processes of meso-scale, dynamic auroral forms. *Space Science Reviews*, *216*(4), 46. https://doi.org/10.1007/s11214-020-00665-y

Gabrielse, C., Angelopoulos, V., Harris, C., Artemyev, A., Kepko, L., & Runov, A. (2017). Extensive electron transport and energization via multiple, localized dipolarizing flux bundles. *Journal of Geophysical Research: Space Physics*, *122*(5), 5059–5076. https://doi.org/10.1002/2017JA023981

Gkioulidou, M., Wang, C. P., Wing, S., Lyons, L. R., Wolf, R. A., & Hsu, T. S. (2012). Effect of an mlt dependent electron loss rate on the magnetosphere-ionosphere coupling. *Journal of Geophysical Research*, *117*(A11). https://doi.org/10.1029/2012JA018032

Henderson, M. G. (1994). *Implications of viking imager results for substorm models*. PRISM. https://doi.org/10.11575/PRISM/10182

Henderson, M. G. (2009). Observational evidence for an inside-out substorm onset scenario. *Annales Geophysicae*, *27*(5), 2129–2140. https://doi.org/10.5194/angeo-27-2129-2009

Henderson, M. G., Reeves, G. D., & Murphree, J. S. (1998). Are north-south aligned auroral structures an ionospheric manifestation of bursty bulk flows? *Geophysical Research Letters*, *25*(19), 3737–3740. https://doi.org/10.1029/98GL02692

Kauristie, K., Sergeev, V. A., Pulkkinen, T. I., Pellinen, R. J., Angelopoulos, V., & Baumjohann, W. (1996). *Study on the ionospheric signatures of the plasma sheet bubbles*. In E. J. Rolfe & B. Kaldeich (Eds.), (Vol. 389, p. 93).

Kivelson, M. G., Kaye, S. M., & Southwood, D. J. (1980). *The physics of plasma injection events*. In S.-I. Akasofu (Ed.), (pp. 385–405).

Liu, J., Angelopoulos, V., Chu, X., Zhou, X.-Z., & Yue, C. (2015). Substorm current wedge composition by wedgelets. *Geophysical Research Letters*, *42*(6), 1669–1676. https://doi.org/10.1002/2015GL063289

Liu, J., Angelopoulos, V., Runov, A., & Zhou, X.-Z. (2013). On the current sheets surrounding dipolarizing flux bundles in the magnetotail: The case for wedgelets. *Journal of Geophysical Research: Space Physics*, *118*(5), 2000–2020. https://doi.org/10.1002/jgra.50092

Liu, W. W., Liang, J., Donovan, E. F., Trondsen, T., Baker, G., Sofko, G., et al. (2008). Observation of isolated high-speed auroral streamers and their interpretation as optical signatures of alfvén waves generated by bursty bulk flows. *Geophysical Research Letters*, *35*(4), L04104. https://doi.org/10.1029/2007GL032722

McIlwain, C. E. (1974). *Substorm injection boundaries*. In B. M. McCormac (Ed.), (pp. 143–154). Springer Netherlands.

Mende, S. B., Harris, S. E., Frey, H. U., Angelopoulos, V., Russell, C. T., Donovan, E., et al. (2008). The themis array of ground-based observatories for the study of auroral substorms. *Space Science Reviews*, *141*(1–4), 357–387. https://doi.org/10.1007/s11214-008-9380-x

Miyashita, Y., Seki, K., Sakaguchi, K., Hiraki, Y., Nosé, M., Machida, S., et al. (2020). On the transition between the inner and outer plasma sheet in the earth's magnetotail. *Journal of Geophysical Research: Space Physics*, *125*(4), e2019JA027561. https://doi.org/10.1029/2019JA027561

Nakamura, R., Baumjohann, W., Klecker, B., Bogdanova, Y., Balogh, A., Rème, H., et al. (2002). Motion of the dipolarization front during a flow burst event observed by cluster. *Geophysical Research Letters*, *29*(20), 3–4. https://doi.org/10.1029/2002GL015763

Nakamura, R., Baumjohann, W., Schödel, R., Brittnacher, M., Sergeev, V. A., Kubyshkina, M., et al. (2001). Earthward flow bursts, auroral streamers, and small expansions. *Journal of Geophysical Research*, *106*(A6), 10791–10802. https://doi.org/10.1029/2000JA000306

Nakamura, R., Oguti, T., Yamamoto, T., & Kokubun, S. (1993). Equatorward and poleward expansion of the auroras during auroral substorms. *Journal of Geophysical Research*, *98*(A4), 5743–5759. https://doi.org/10.1029/92JA02230

Pritchett, P. L., Coroniti, F. V., & Nishimura, Y. (2014). The kinetic ballooning/interchange instability as a source of dipolarization fronts and auroral streamers. *Journal of Geophysical Research: Space Physics*, *119*(6), 4723–4739. https://doi.org/10.1002/2014JA019890

Rostoker, G., Lui, A. T. Y., Anger, C. D., & Murphree, J. S. (1987). North-south structures in the midnight sector auroras as viewed by the viking imager. *Geophysical Research Letters*, *14*(4), 407–410. https://doi.org/10.1029/GL014i004p00407

Runov, A., Angelopoulos, V., Gabrielse, C., Zhou, X. Z., Turner, D., & Plaschke, F. (2013). Electron fluxes and pitch-angle distributions at dipolarization fronts: Themis multipoint observations. *Journal of Geophysical Research: Space Physics*, *118*(2), 744–755. https://doi.org/10.1002/jgra.50121

Runov, A., Angelopoulos, V., Sitnov, M. I., Sergeev, V. A., Bonnell, J., McFadden, J. P., et al. (2009). Themis observations of an earthward-propagating dipolarization front. *Geophysical Research Letters*, *36*(14), L14106. https://doi.org/10.1029/2009GL038980

Russell, C. T., Chi, P. J., Dearborn, D. J., Ge, Y. S., Kuo-Tiong, B., Means, J. D., et al. (2008). Themis ground-based magnetometers. *Space Science Reviews*, *141*(1–4), 389–412. https://doi.org/10.1007/s11214-008-9337-0

Sato, N., Kadokura, A., Motoba, T., Hosokawa, K., Bjornsson, G., & Saemundsson, T. (2012). Ground-based aurora conjugacy and dynamic tracing of geomagnetic conjugate points. *Auroral Phenomenology and Magnetospheric Processes: Earth And Other Planets*, *91–98*. https://doi.org/10.1029/2011GM001154

Sato, N., Kadokura, A., Motoba, T., Hosokawa, K., Björnsson, G., & Saemundsson, T. (2015). Interhemispheric symmetries and asymmetries of aurora from ground-based conjugate observations. *Auroral Dynamics and Space Weather*, 145–161. https://doi.org/10.1002/9781118978719.ch11

Sergeev, V. A., Liou, K., Meng, C. I., Newell, P. T., Brittnacher, M., Parks, G., & Reeves, G. D. (1999). Development of auroral streamers in association with localized impulsive injections to the inner magnetotail. *Geophysical Research Letters*, *26*(3), 417–420. https://doi.org/10.1029/1998GL900311

Sergeev, V. A., Sauvaud, J. A., Popescu, D., Kovrazhkin, R. A., Liou, K., Newell, P. T., et al. (2000). Multiple-spacecraft observation of a narrow transient plasma jet in the earth's plasma sheet. *Geophysical Research Letters*, *27*(6), 851–854. https://doi.org/10.1029/1999GL010729

Singer, H., Matheson, L., Grubb, R., Newman, A., & Bouwer, D. (1996). *Monitoring space weather with the goes magnetometers*. In E. R. Washwell (Ed.), (Vol. 2812, p. 299–308). https://doi.org/10.1117/12.254077

Tian, S. (2022). Moon and background removal algorithm for all-sky imager. arXiv. https://doi.org/10.48550/ARXIV.2205.10882

Torr, M. R., Torr, D. G., Zukic, M., Johnson, R. B., Ajello, J., Banks, P., et al. (1995). A far ultraviolet imager for the international solar-terrestrial physics mission. *Space Science Reviews*, *71*(1–4), 329–383. https://doi.org/10.1007/BF00751335

Tsyganenko, N. A. (1989). A magnetospheric magnetic field model with a warped tail current sheet. *Planetary and Space Science*, *37*(1), 5–20. https://doi.org/10.1016/0032-0633(89)90066-4

Vanhamäki, H., & Juusola, L. (2020). *Introduction to spherical elementary current systems*. Springer International Publishing. https://doi.org/10.1007/978-3-030-26732-2_2

Wang, C.-P., Gkioulidou, M., Lyons, L. R., & Wolf, R. A. (2018). Spatial distribution of plasma sheet entropy reduction caused by a plasma bubble: Rice convection model simulations. *Journal of Geophysical Research: Space Physics*, *123*(5), 3380–3397. https://doi.org/10.1029/2018JA025347

Wang, C.-P., Lyons, L. R., Weygand, J. M., Nagai, T., & McEntire, R. W. (2006). Equatorial distributions of the plasma sheet ions, their electric and magnetic drifts, and magnetic fields under different interplanetary magnetic field bz conditions. *Journal of Geophysical Research*, *111*(A4), A04215. https://doi.org/10.1029/2005JA011545

Wang, C.-P., Yang, J., Gkioulidou, M., Lyons, L. R., & Wolf, R. A. (2020). Generation and evolution of two opposite types of mesoscale plasma sheet bubbles. *Journal of Geophysical Research: Space Physics*, *125*(9), e2020JA028072. https://doi.org/10.1029/2020JA028072

Weygand, J. M. (2009a). Equivalent ionospheric currents (eics) derived using the spherical elementary currents systems (secs) technique at 10 sec resolution in geographic coordinates. *UCLA*. https://doi.org/10.21978/P8D62B

Weygand, J. M. (2009b). Spherical elementary current (sec) amplitudes derived using the spherical elementary currents systems (secs) technique at 10 sec resolution in geographic coordinates. https://doi.org/10.21978/P8PP8X

Weygand, J. M., Amm, O., Viljanen, A., Angelopoulos, V., Murr, D., Engebretson, M. J., et al. (2011). Application and validation of the spherical elementary currents systems technique for deriving ionospheric equivalent currents with the north American and Greenland ground magnetometer arrays. *Journal of Geophysical Research*, *116*(A3). https://doi.org/10.1029/2010JA016177

Weygand, J. M., Bortnik, J., Chu, X., Cao, X., Li, J., Aryan, H., & Tian, S. (2022). Magnetosphere-ionosphere coupling between north-south propagating streamers and high-speed earthward flows. *Journal of Geophysical Research: Space Physics*, *127*(10), e2022JA030741. https://doi.org/10.1029/2022JA030741

Zesta, E., Lyons, L. R., & Donovan, E. (2000). The auroral signature of earthward flow bursts observed in the magnetotail. *Geophysical Research Letters*, *27*(20), 3241–3244. https://doi.org/10.1029/2000GL000027